Tackling the phylogenetic conundrum of Hydroidolina (Cnidaria: Medusozoa: Hydrozoa) by assessing competing tree topologies with targeted high-throughput sequencing.

Bastian Bentlage[1,*], Allen G. Collins[2]

[1]Marine Laboratory, University of Guam, 303 University Dr., Mangilao, GU 96913, USA

[2]National Museum of Natural History & National Systematics Laboratory of NOAA's Fisheries Service, Smithsonian Institution, Washington DC, USA

*Correspondence: bentlageb@triton.uog.edu

Abstract

Higher-level relationships of the Hydrozoan subclass Hydroidolina , which encompasses the vast majority of medusozoan cnidarian species diversity, have been elusive to confidently infer. The most widely adopted phylogenetic framework for Hydriodolina based on ribosomal RNA data received low support for several higher level relationships. To address this issue, we developed a set of RNA baits to target more than a hundred loci from the genomes of a broad taxonomic sample of Hydroidolina for high-throughput sequencing. Using these data, we inferred the relationships of Hydroidolina using maximum likelihood and Bayesian approaches. Both inference methods yielded well-supported phylogenetic hypotheses that largely agree with each other. Using maximum likelihood and Baysian hypothesis testing frameworks, we found that several alternate topological hypotheses receive strong support in light of the genomic data generated for this study. Nonetheless, the Bayesian topology proposed herein consistently scores well across testing frameworks, suggesting that it represents the most likely phylogenetic hypothesis of Hydroidolina. The Bayesian posterior topology infers Aplanulata as earliest branching lineage of Hydroidolina. This is a strong deviation from previous phylogenetic analyses that placed Capitata or Siphonophorae as earliest branching lineages of Hydroidolina. Considering that Aplanulata represents a lineage comprised of species that for the most part possess a life cycle involving a solitary polyp and free-swimming medusa stage, the phylogenetic hypotheses presented herein have potentially far-reaching implications for our understanding of the evolution of life cycles, coloniality, and the division of labor in Hydrozoa.

Introduction

While the fossil record of medusozoan cnidarians is scant, the origin of the group has been inferred to lie near the end of the Ediacaran, approximately 550-580 million years ago (Han et al., 2016). Plausible crown-group hydrozoans have been described from some 500 million year old Cambrian deposits (Cartwright et al., 2007), suggesting an ancient origin of extant hydrozoans likely dating back to the

period of rapid diversification of metazoan life during which all major modern animal phyla emerged (Valentine et al., 1999; Erwin, 2020). Hydrozoans are of particular interest in the study of the evolution of development, as their radiation gave rise to diverse life cycle strategies, diverse forms of coloniality and the division of labor (Cartwright & Nawrocki, 2010; Bentlage et al., 2018; Cartwright et al., 2020). This diversity is concentrated in the hydrozoan subclass Hydroidolina, the most speciose medusozoan clade which contains the vast majority of the 3,800 nominal hydrozoan species (Daly et al., 2007; Schuchert, 2020). Elucidating the evolutionary history and patterns of complex character evolution in Hydroidolina requires a solid understanding of the phylogenetic history of the group (e.g., Cartwright et al., 2020).

However, the goal of inferring the deep phylogeny of Hydroidolina has been elusive, possibly as a result of the early origin and likely rapid diversification of the group. The most comprehensive phylogenetic hypothesis (Cartwright & Nawrocki, 2010) of higher-level relationships within Hydroidolina was inferred using ribosomal DNA (rDNA) from a broad taxonomic sample. While shallow nodes were well resolved with high confidence, higher-level relationships generally received weak support. In particular, Capitata, Siphonophorae, and Aplanulata were inferred to be monophyletic groups while Filifera was polyphyletic (Cartwright et al., 2008; Cartwright & Nawrocki, 2010), Previously, these four taxa were united under the name Anthoathecata but their non-monophyly had been demonstrated earlier (Collins et al., 2006). The other major hydroidolinan clade, Leptothecata was inferred monophyletic (Collins et al., 2006; Cartwright et al., 2008; Cartwright & Nawrocki, 2010), consistent with more traditional taxonomic treatments. Whole mitochondrial genomes have been employed previously to address this issue and to reconstruct deep nodes within the phylogeny of Hydroidolina (Kayal et al., 2015). While this approach led to a well-resolved and highly supported phylogenetic hypothesis, several nodes of the resulting tree topology are at odds with rDNA-based phylogenies (Cartwright et al. 2008; Cartwright & Nawrocki, 2010) and recent phylogenomics-based hypotheses (Kayal et al. 2018).

Recent improvements in the understanding of medusozoan, and more broadly cnidarian relationships, were made by employing phylogenomic datasets derived from whole-transcriptome and genome-sequencing efforts (Zapata et al., 2015; Kayal et al., 2018). While these efforts provided answers to several long-standing questions of cnidarian evolutionary history, taxon sampling was limited, preventing rigorous evaluation of hydrozoan relationships. We used the coding sequences generated by these phylogenomic studies as a backbone for targeted high-throughput sequencing, producing a multi-locus dataset to infer the phylogeny of Hydroidolina. For this purpose, we developed a set of custom baits to enrich target loci from a representative sample of hydroidolinan hydrozoans. This work provides a new framework for the phylogeny of Hydroidolina that will enable further phylogenetic comparative studies of character evolution in Hydrozoa. To evaluate multiple competing topological hypotheses of hydroidolinan relationships, both likelihood and Bayesian statistical frameworks (cf. Sober, 2008) were employed to discriminate between alternate tree topologies and evaluate the strength of evidence supporting prior phylogenetic hypotheses of Hydroidolina as well as those phylogenies inferred from the multi-locus dataset presented here.

Materials and Methods

Bait design for targeted sequencing

Biotinylated RNA baits of 120bp length were designed using 355 orthogroup partitions (loci) from the phylogenomic OF-PTP_75tx matrix (Kayal et al., 2018). This dataset contains the coding sequences from a broad taxonomic sample of cnidarians, including anthozoans, medusozoans, and endocnidozoans. Due to their large sequence divergences, endocnidozoans were excluded from the dataset used for RNA bait design. Nucleotide sequences were aligned per locus guided by their predicted amino acid translations using the Geneious aligner (version 9; Biomatters, Auckland, New Zealand). Several sequences were flagged after manual audit of alignments due to their apparent divergence and identified as non-homologous sequences after BLAST searches against NCBI's

GenBank. Following curation and removal of sequences shorter than 80bp, putative repetitive elements in the remaining 5,523 sequences were soft-masked using the cross_match search option against the Cnidaria repeats database in RepeatMasker (version 4.06; Smit et al., 2013-2015).

Next, sequence stretches of 10 or fewer ambiguous nucleotides (N) were replaced with thymine (T) repeats to allow bait design across short regions of undetermined sequences. Similarly, short sequences less than 120bp were padded with T repeats to allow for 120bp long baits to be mapped against reference sequences. Baits were designed at approximately 2.5x tiling density with some 50bp spacing between the start of neighboring baits, yielding 38,102 candidate baits. Each candidate bait was verified against six cnidarian genome assemblies (Table 1) using BLAST searches to evaluate its fit to the reference. Hits with a length greater than 45bp in length and identity greater than 75% were retained for further analysis. Melting temperatures (Tm; defined as the temperature at which 50% of molecules hybridize) were estimated for each BLAST hit assuming standard Mybaits (Mycroarray, Arbor Biosciences, Ann Arbor, MI, USA) hybridization conditions. Based on the distribution of inferred Tms, baits of moderate or higher specificity were retained. That is, candidate baits with at most 10 BLAST hits between 62.5°C to 65°C, two BLAST hits above 65°C, and fewer than 2 baits on each flanking region were retained, yielding a total of 37,546 baits (Supplementary File 1).

Target capture and sequencing

Genomic DNA was extracted from ethanol-preserved tissue samples (Table 2) using a standard organic phenol-chloroform extraction protocol (Green & Sambrook, 2012). Extracted DNA was quantified with a Qubit 4 fluorometer (Thermo Fisher Scientific, Waltham, MA, USA). 50µl of DNA in TE buffer were chilled to 4˚C in the water bath of a Q800 Sonicator (Qsonica, Newton, CT, USA) and acoustically sheared for nine minutes using an amplitude of 25 with sonication pulses of 15s on/15s off. Illumina sequencing libraries were constructed from sheared DNA samples using an NEBNext Ultra II DNA library preparation kit (New England Biolabs, Ipswich, MA, USA) with dual indexes for multiplexing

following the manufacturer's protocol. After library amplification and magnetic bead purification using Ampure beads (Promega, Madison, WI, USA), amplicons longer or shorter than approximately 200bp were removed using a BluePippin size select gel eletrophoresis system (Sage Science, Beverly, MA, USA). Concentrations of size-selected libraries were equilibrated, followed by pooling of libraries three to four samples deep for target enrichment.

Hybridization of RNA baits to pooled libraries followed the Mybaits version 3.02 protocol (Mycroarray, Arbor Biosciences, Ann Arbor, MI, USA) with the following modifications. After initial denaturation and blocking with Illumina adapter-specific oligonucleotides, RNA baits were allowed to hybridize for 19 hours at 65˚C, 19 hours at 60˚C, and 10 hours at 55˚C. We used this touchdown procedure on the newly and developed untested bait set in an effort to increase on-target specificity while allowing for sensitivity of reactions. Following hybridization, biotinylated baits were bound to streptavidin-coated magnetic beads (Dynabeads MyOne Streptavidin; Thermo Fisher Scientific, Waltham, MA, USA), followed by stringent washing to remove unbound DNA library molecules. Captured libraries were amplified while bound to beads using KAPA HiFi DNA polymerase and HotStart ReadyMix (Roche, Basel, Switzerland) following the manufacturers protocol. The annealing temperature during the 15 amplification cycles was 60˚C. PCR reactions were cleaned using Ampure magentic beads (Thermo Fisher Scientific, Waltham, MA, USA), washing twice with 80% ethanol. DNA concentrations were quantified fluorometrically, followed by equilibration of target-enrichment pools to equimolar concentrations. All reactions were pooled and the size range of the pool selected for an average length of 450bp using the BluePippin size select system (Sage Science, Beverly, MA, USA). Following quantification using qPCR, 300bp paired-end reads were generated on the Illumina MiSeq platform with the v3 reagent kit (Illumina, San Diego, CA, USA).

Sequence assembly and alignment

Sequencing adapters were removed from paired-end sequencing reads using Trimmomatic (version 0.22; Bolger et al., 2014). Reads were trimmed further using a sliding window of size four, with an average quality of 15 or greater for the bases within the window to be retained. Quality trimmed reads shorter than 75bp were discarded. The HybPiper pipeline (version 1.2; Johnson et al., 2016) was used to identify target sequences from enriched sequencing libraries by comparing all quality trimmed reads against the cnidarian reference protein collection from Kayal et al. (2018) using translated BLAST queries. After extraction of target reads and binning by locus, reads were assembled for each species using the SPAdes assembler (version 3.10.1; Bankevich et al., 2012), followed by alignment and scaffolding of contigs against the reference proteins using Exonerate (version 2.2.0; Slater & Birney, 2005). In-frame coding sequences of scaffolds (super-contigs) were translated into amino acids. All loci were individually aligned using MAFFT (version 7.271; Katoh & Standley, 2013) and ambiguous alignment positions were removed using Gblocks (version 0.91b; Talavera & Castarena, 2007) via Gblockwrapper (version 0.03; https://goo.gl/fDjan6). Following alignment and removal of ambiguous alignment positions, all loci were concatenated.

Phylogenetic inference

Phylobayes (version 4.1c; Lartillot et al., 2013) was used to run eight independent MCMC chains and the posterior probability distribution was sampled until chains converged and a large sample of trees was generated. To account for site-specific differences in the evolutionary rates within and among alignment partitions, site-specific rates were inferred from the data using the CAT-GTR model during MCMC runs (Lartillot & Philippe, 2004). PartitionFinder (version 2.1.1; Lanfear et al., 2017) was used to determine the best partitioning scheme for the concatenated alignment, with maximum likelihood phylogenetic trees during partitioning analysis inferred using RAxML (version 8.2.12; Stamatakis, 2006). In the absence of prior information on possible partitioning schemes, the relaxed clustering algorithm (rclusterf; Lanfear et al., 2014) was used to identify partitioning schemes that fit the data

well. Initial clustering analyses included all substitution models implemented in PartitionFinder. These exploratory analyses failed to finish after more than a month of run-time but indicated that models with rate heterogeneity modeled by drawing from the gamma distribution (+G) and amino acid residue equilibrium frequencies estimated from the data (+F) fit data partitions best. Due to their prevalence in preliminary results and tractability of partitioning analysis, the final partitioning scheme was inferred using the LG (Le & Gascuel, 2008), WAG (Wheelan & Goldman, 2001), and MtZoa (Rota-Stabelli et al., 2009) substitution matrices. The resulting partitioning scheme was used to infer the maximum likelihood phylogeny using RAxML (Stamatakis, 2006). The best tree was chosen from a set of 10 trees inferred from independent searches, starting from different random starting trees. Robustness of the resulting maximum likelihood phylogeny was assessed using 681 non-parametric bootstrap replicates.

Tree topology hypothesis testing

Given a set of constraints to fix overall tree topologies according to previous phylogenetic hypotheses of Hydroidolina (Cartwright and Nawrocki 2010, Kayal et al. 2015) and the set of trees inferred herein, phylogenetic analyses were conducted in both maximum likelihood and Bayesian frameworks. Tree space for topological hypothesis tests were constrained in a manner to set informative priors on tree searches (Bergstein et al., 2013). In short, the backbone nodes of each tree, including the best trees found in unconstrained searches, were fixed. Tree inferences were able to rearrange the topology of unconstrained nodes and make adjustments to branch lengths to maximize the likelihood of the tree given the data in the concatenated amino acid residue alignment. Constrained maximum likelihood phylogenies were reconstructed using 10 independent partitioned RAxML searches, retaining the tree with the highest log likelihood (lnL). Samples of the Bayesian posterior probability distribution were obtained from eight independent MCMC chains under the CAT-GTR model implemented in PhyloBayes, as described under phylogenetic inference above.

Cartwright & Nawrocki's (2010) phylogeny represents the phylogenetic framework for Hydroidolina most widely adopted and was thus used as the null hypothesis (T_0) against which all alternate trees were evaluated quantitatively using the likelihood ratio. The likelihood ratio statistic was calculated as

$$\delta\text{lnL} = 2(\text{lnL } T_A - \text{lnL } T_0)$$

where lnL T_0 represents the likelihood of the tree under the null hypothesis and lnL T_A the likelihood of the tree under the alternate hypothesis. Here, a negative δlnL indicates a better fit of T_0 to the data while a positive δlnL indicates that T_A explains the data better. Resampling of site log likelihoods (RELL; Kishino et al., 1990; Hasegawa & Kishino, 1994) was used to generate 10,000 bootstrap samples for each tree hypothesis, estimating the variance of tree likelihoods. Using these RELL bootstrap distributions, the null hypothesis that trees of the candidate set have the same lnL was tested via the approximately unbiased test (AU; Shimodaira, 2002), as implemented in Consel (version 0.2; Shimodaira & Hasegawa, 2001). Phylogenetic tree fit to the data was further evaluated using the posterior probability of all candidate trees using the Bayesian Information Criterion (BIC; Schwarz, 1978) approximation implemented in Consel.

Bayes factors (reviewed in Morey et al., 2016) were calculated to compare the model (tree) with the highest posterior lnL to all other models (trees) in pairwise comparisons. These comparisons address the question of how well the best tree hypothesis predicts the observed amino acid alignment compared to the alternate tree hypotheses. Bayesian model evaluation requires quantifying model evidence by a marginal likelihood function through integration of the product of the likelihood and the prior (Fourment et al., 2020). Model comparisons with Bayes factors use ratios of marginalized likelihoods, which are difficult to compute exactly. To address this issue, the harmonic mean of the posterior is widely used as an estimator of the marginal likelihood (Kass & Raftery, 1995). Combining the posterior distributions of eight MCMC chains for a given constrained tree search, we calculated the moving harmonic mean of the posterior using a sliding window with a step length of one and a size

equal to the current cycle of the MCMC cycle times 0.1. The natural logarithm of the ratio of harmonic means was used for tree comparisons and interpreted following a modified version of Jeffreys' (1961) categories of evidence (cf. Kass and Raftery, 1995). In particular, Bayes factors were calculated as

$$BF_{A0} = 2 * \ln(\ln L\ T_A - \ln L\ T_0)$$

where $\ln L\ T_0$ is the marginal likelihood of the MCMC search under the null hypothesis and T_A the marginal likelihood of the alternate MCMC tree search. Note that the likelihood ratio may be negative leading to an undefined result of the logarithmic function, an issue we took into account by taking the absolute of the ratio if negative, followed by multiplying the resulting Bayes factor by negative one.

Results

Recovery of target loci and alignment

The final concatenated alignment (Fig. 1A) contained 44 medusozoan cnidarians, sequence data for 18 of which were generated in this study (Table 2). This alignment contained 134 of the 355 targeted loci, with a total alignment length of 21,816 character columns. Loci targeted but not included in the final alignment failed to generate sequence data from target enrichment reactions and were excluded from further analysis. Alignment lengths per locus ranged from 56 to 363 positions (average 164), with a combined total of 333 to 5,818 (average 2,891) amino acids contained in each alignment (Fig. 1B). Taxon occupancy per locus ranged from 5 to 36 species with an average of 21 species included in each alignment partition for phylogenetic analysis (Fig. 1C). Among ingroup hydrozoans, coverage varied between and within clades, with matrix completeness being highest for taxa of the Kayal et al. (2018) reference dataset (Fig. 1A; Table 4). In particular, sequence data for Aplanulata, Siphonophorae, and Filifera III largely represent previously published sequence data that were used for bait design (Table 2). Consequently, alignment coverage in these groups ranges from some 40% to almost 80%. Despite being closely related to at least some of the taxa used in bait design, success in recovering loci from *Podocoryne martinicana* (Filifera III) and *Athorybia rosacea* (Siphonophorae) was limited (Table 2).

In species of Filifera I, Filifera II, and Capitata target capture yields ranged from as few as some 500 amino acid residues spread over five loci (*Myrionema hargitti*) to as high as some 4,400 residues contained in 46 separate loci (*Pennaria disticha*). By contrast, the RNA bait set and hybridzation protocol employed here was highly successful in recovering sequence data for leptothecate hydrozoans despite being somewhat distantly related to any of the reference taxa. On average, 49 target loci comprising close to 5,000 amino acid residues were recovered for leptothecate species (Table 2). Here, the maximum yield was some 8,000 residues spread across 80 separate loci (*Kirchenpaueria* sp.).

Phylogeny of Hydroidolina inferred from target-capture sequencing

Bayesian MCMC chains using the CAT-GTR model were terminated after some 14,000 iterations, of which the first 3,000 were discarded as burn-in. Chains were thinned by sampling every tenth generation, yielding a mean difference between chains of 9e-4 and a maximum difference of 0.0469. The majority rule consensus of the posterior shows a well-resolved phylogeny with high posterior probabilities for the monophyly of the major ingroup and outgroup clades (Fig. 2). Aplanulata represents the earliest branching lineage of Hydroidolina. As in previous analyses, Filifera represents a polyphyletic taxon. Interestingly, Filifera I plus II are each other's closest relative as are Filifera III plus IV. Filifera I plus II are the closest relatives to Capitata, albeit with a posterior probability slightly less than 0.95; Leptothecata is inferred as sister to the clade of Filifera I plus II and Capiata. Filifera III plus IV are the closest relatives of Siphonophorae.

For ML phylogenetic inference, the best partitioning scheme of the 134 locus dataset contained 25 partitions. In particular, the ML phylogeny was inferred using 22 partitions comprising 128 loci under the LG+G+F model, two partitions with a total of 5 loci under the MTZOA+G+F model, and 1 partition with a single locus under the WAG+G+F model. The ML tree largely agrees with the Bayesian inference (Fig. 2), but differs in the placement of Filifera I plus II relative to Capitata and Leptothecata. In contrast to the Bayesian inference, Filifera I plus II are the sister to Leptothecata rather

than Capitata. However, this result lacks support with a bootstrap of less than 50. While the majority of the other nodes in both the in- and outgroup received high bootstrap support, the deep ingroup node uniting Filifera III plus IV and Siphonophorae is weakly supported with a bootstrap of 65. Despite these differences between Bayesian and ML phylogenies, both analyses agree in confidently inferring Aplanulata to be the earliest branching lineage of Hydroidolina.

Phylogenetic hypothesis testing

Phylogenies were inferred under six different constraints (Fig. 3A). Two phylogenies, T_0 (cf. Cartwright & Nawrocki, 2010) and T_1 (cf. Kayal et al., 2015), were rejected by the AU test (Table 3). Interestingly, T_0 had a higher likelihood than T_1, a fact reflected in a likelihood ratio of approximately -200, indicating a far worse fit of T_1 to the data compared to T_0. T_2 and T_3 were constrained following the Bayesian and Maximum likelihood phylogenies inferred herein. Both tree hypotheses are roughly equally likely, with the maximum likelihood phylogeny being a slightly better fit to the data (Table 2). Both T_2 and T_3 (Fig. 3) have a much better fit to the data than T_0 (likelihood ratio greater than 200; Table 2). T_4 and T_5 (Fig. 3) were included in the tree set to be evaluated to account for the low bootstrap support received for the placement of Siphonophorae and Filifera III plus IV (Fig. 2). Neither T_4 nor T_5 were rejected by the AU test, but their BIC posterior probabilities are extremely small. Interestingly, both T_4 and T_5 contain a sister-group relationship between Capitata and Filifera I plus II, similar to the results of the Bayesian tree inference.

Constrained Bayesian searches found the marginal likelihood of T_2 to be much higher than the marginal likelihood of T_0 (Fig. 3B) providing strong evidence that T_2 is better at predicting the data than T_0 (BF_{20} = 8.4; Fig. 3C). Similar to the results of the AU test, the Bayesian analysis provides strong evidence for T_4 (BF_{40} = 9.1) and T_5 (BF_{50} = 7.4) over T_0. Surprisingly, the Bayes Factor analysis strongly favors T_0 over the maximum likelihood tree T_3 (BF_{30} = -7.7). By contrast, the Kayal et al. (2015) tree T_1 scores

the highest marginal likelihoods of all tree searchers after almost 16,000 MCMC generations and is strongly favored over T_0 ($BF_{10} = 10.5$).

Discussion

A new phylogenetic hypothesis for Hydroidolina

Despite highly variable recovery rates of target loci that leave large gaps in the final alignment (Fig. 1A), the dataset analyzed here provides high resolution of the deep phylogeny of Hydroidolina. While missing data could affect tree topology inference, in practice accurately placing taxa despite missing information is often not a major concern (Wiens et al., 2011). Indeed, we were able to infer a well-resolved phylogeny by combining a publicly available data-rich amino acid sequence dataset with new data from key hydrozoan taxa that have so far been absent from multi-gene phylogenomic datasets. Overall topologies recovered in our phylogenetic inferences are consistent with previous phylogenomic analyses (Zapata et al., 2015; Kayal et al., 2018). While neither Zapata et al. (2015) nor Kayal et al. (2018) included sufficient taxa representing Hydroidolina to allow for much insight into the evolutionary history of the group, both recovered Aplanulata as the earliest diverging hydroidolinan clade, a placement we confirmed after comprehensively sampling higher-level taxa of Hydroidolina (Fig. 2). This placement is at odds with previous phylogenetic treatments of Hydroidolina that inferred a more recent origin of Aplanulata within Hydroidolina as sister of Filifera I plus II (Cartwright & Nawrocki, 2010; Kayal et al., 2015). Placing Aplanulata as the earliest branching member of Hydroidolina has potentially far-reaching consequences for our understanding of hydrozoan evolution. Aplanulata is dominated by solitary polyp-forming taxa, a trait common in other medusozoans but rare across Hydroidolina in which colonial hydroids, many of which are polymorphic, displaying a reproductive division of labor, dominate (Cartwright & Nawrocki, 2010; Cartwright et al., 2020).

Ingroup relationships within Hydroidolina appear largely congruent across the Bayesian posterior tree set and the maximum likelihood phylogeny with the exception of the placement of Filifera I plus II

with respect to Capitata and Leptothecata (Fig. 2). One possible explanation for this disagreement may be that the substitution matrix-based models used for maximum likelihood inference here are potentially less accurate in reflecting the substitution process that led to the observed data. Exploratory partitioning analyses with PartitionFinder suggested that substitutions in a significant number of partitions should be inferred using the GTR model. However, benchmarking of partitioning analyses under the GTR model indicated that computational time would be prohibitive to search across this large parameter space. To address this issue, partitioning schemes were inferred using simpler substitution matrices (i.e., LG, WAG, and MtZoa). Regardless of this poorly supported topological difference in the placement of Filifera I plus II (Fig. 2), the overall relationships recovered are consistent across analyses but at odds with previous phylogenetic hypotheses of Hydroidolina (cf. Cartwright & Nawrocki, 2010; Kayal et al., 2015). Despite conflicts between the phylogenetic hypotheses presented here and previous treatments of Hydroidolina, a consistent result that has emerged over the last decade is the polyphyly of Filifera. In agreement with prior phylogenetic hypotheses (Cartwright & Nawrocki, 2010; Kayal et al., 2015), we find that Filifera I plus II forms a monophyletic clade as does Filifera III plus IV. As of now, these clades remain without clear definition based on morphological or life history characteristics.

Phylogenetic tree selection

To facilitate discriminating between competing hypotheses of hydroidolinan relationships, we quantified the evidence for the set of alternate phylogenetic hypotheses (Fig. 3A) in light of the multi-locus dataset analyzed here. Simple likelihood ratios (Table 3) indicate that T_0 (Fig. 3A; Cartwright & Nawrocki, 2010) is a better fit than the mitochondrial genome-based phylogenetic hypothesis T_1 (Kayal et al., 2015). However, neither T_0 nor T_1 fit the data well compared to any of the alternate hypotheses derived from the phylogenetic framework proposed herein (T_3-T_5; Fig. 3A). Indeed, T_0 and T_1 are rejected by the AU test while T_2-T_5 cannot be rejected. However, the majority rule consensus of the

Bayesian posterior (T_2) and the maximum likelihood topology (T_3) receive high BIC-based posterior probabilities compared to the very small posterior probabilities of the alternate hypotheses (Table 3).

The hypothesis tests above reduce the set of credible trees by eliminating several unlikely tree topologies. However, the procedures employed rely on the likelihood of a single phylogeny, implicitly assuming that the tree is known without error. Resampling of site likelihoods from this best tree is used to estimate variances of tree likelihoods for comparisons. Bayesian approaches that estimate the posterior probability distribution of phylogenetic hypotheses allow averaging across tree topologies and branch lengths for more comprehensive incorporation of uncertainty into comparisons of phylogenetic trees. Bayes factors incorporate these uncertainty estimates in model comparisons by employing ratios of marginal likelihoods. Bayes factors allowed us to quantify the weight of evidence for a given topological hypothesis. We found that T_2 predicts the alignment data best compared to the null, T_0 (Fig. 3B). Similarly, T_4 and T_5, both of which represent variations of T_2 that differ in their placement of Siphonophorae (Fig. 3A), predict the alignment data better than does T_0 (Fig. 3B).

Surprisingly, the phylogenetic relationships proposed by Kayal et al. (2015; T_1) based on whole mitochondrial genomes received the highest marginal likelihoods (Fig. 3A), being favored over both T_0 and T_2 (Fig. 3B). T_1 places Siphonophorae as the earliest branching lineage within Hydroidolina. This mitochondrial genome-based phylogenetic hypothesis has so far been widely disregarded by the scientific community, likely as a result of the understanding that mitochondrial DNA exhibits generally higher substitution rates than nuclear DNA. High substitution rates may lead to sequence saturation and consequently homoplasy that may obscure phylogenetic signal and produce highly supported, but misleading phylogenies across deep divergences (Rubinoff & Holland, 2005). However, the alignment used here only contained five mitochondrial loci compared to 134 nuclear loci.

Despite no single phylogenetic hypothesis being identified as fitting the data best by either maximum likelihood or Bayesian hypothesis testing, T_2 (Fig. 2, left) appears to consistently display very high predictive power for the alignment data compared to the null hypothesis T_0 (Table 3; Fig. 3C)

and alternate hypotheses. Consequently, we suggest it as the most viable hypothesis of hydroidolinan relationships to date. That said, further studies with additional taxa and alternative characters are still needed to assess the validity of this working hypothesis.

Conclusions

This study represents one of only a few attempts at using target-enriched high throughput sequencing to generate a multi-locus alignment for phylogenetic analyses of Cnidaria. Previous attempts had been limited to Anthozoa (Quattrini et al., 2018; Erickson et al., 2020), relying on the greater availability of genomic data for Anthozoa compared to Medusozoa. Despite mixed success in capturing target loci, we were able to generate an informative multi-gene alignment that produced a well-supported phylogenetic hypothesis for Hydroidolina. One drawback of bait-development based on coding sequences alone, as done here, is that baits may inadvertently be designed across intron-exon boundaries which is likely to reduce bait effectiveness. As availability of genomic resources increases, it will be possible to address these issues and apply target capture sequencing approaches routinely to phylogenetic studies of medusozoan cnidarians, building on the growing knowledge-base for designing targeted high-throughput sequencing experiments (reviewed in Andermann et al., 2020). Nonetheless, we were able to address long-standing questions in hydrozoan phylogenetics by applying relevant constraints (priors) to make informed decisions for discriminating between alternate phylogenetic hypotheses for Hydroidolina. We suggest that T_2 (Fig. 2, left; Fig. 3A) represents the most likely tree topology for hydroidolinan evolutionary relationships to date. While both the likelihood-based AU test (Table 3) and Bayes factors (Fig. 3C) failed to reject several of the alternate topologies, the consistent inclusion of the T_2 topology in the set of phylogenies that perform better at predicting the data compared to the null hypothesis suggests that T_2 is the most viable representation of phylogenetic relationships of Hydroidolina.

Acknowledgements

This work was supported by Guam EPSCoR through NSF award OIA-1457769 and funding by the Small Grants program of the National Museum of Natural History (NMNH), Smithsonian Institution. Part of this work was performed using resources of the Laboratories of Analytical Biology (LAB) at NMNH and we thank LAB staff for valuable advice on laboratory protocols and procedures. BB wishes to acknowledge the numerous discussions with the participants in his bioinformatics and data analysis course that informed many of the analytical approaches for phylogenetic hypothesis testing used here.

References

Andermann T, Torres JMF, Matos-Maraví P, Batista R, Blanco-Pastor JL, Gustafsson ALS, Kistler L, Liberal IM, Oxelman B, Bacon CD, Antonelli A (2020) A guide to carrying out a phylogenomic target sequence capture project. *Frontiers in Genetics* 10:1407.

Bankevich, A., Nurk, S., Antipov, D., Gurevich, A. A., Dvorkin, M., Kulikov, A. S., Lesin, V. M., Nikolenko, S. I., Pham, S., Prjibelski, A. D., Pyshkin, A. V., Sirotkin, A. V., Vyahhi, N., Tesler, G., Alekseyev, M. A., Pevzner, P. A. (2012) SPAdes: A New Genome Assembly Algorithm and Its Applications to Single-Cell Sequencing. *Journal of Computational Biology*, 9: 455-477.

Bayha, K. M., Collins, A. G., & Gaffney, P. M. (2017). Multigene phylogeny of the scyphozoan jellyfish family Pelagiidae reveals that the common U.S. Atlantic sea nettle comprises two distinct species (*Chrysaora quinquecirrha* and *C. chesapeakei*). *PeerJ*, *5*, e3863.

Bentlage B, Osborn KJ, Lindsay DJ, Hopcroft RR, Raskoff KA, Collins AG (2018) Loss of metagenesis and evolution of a parasitic life style in a group of open-ocean jellyfish. *Mol Phyl Evol* 124:50-59.

Bergsten J, Nilsson AN, Ronquist F (2013) Bayesian tests of topology hypotheses with an example from diving beetles. *Systematic Biology* 62:660-673.

Bolger, A. M., Lohse, M., & Usadel, B. (2014). Trimmomatic: A flexible trimmer for Illumina Sequence Data. *Bioinformatics* 30:2114-2120.

Cartwright P, Evans NM, Dunn CW, Marques AC, Miglietta MP, Collins AG. 2008. Phylogenetics of Hydroidolina (Cnidaria, Hydrozoa). *J Mar Biol Assoc* 88:1163–72.

Cartwright P, Halgedahl SL, Hendricks JR, Jarrard RD, Marques AC, Collins AG, Lieberman BS (2007) Exceptionally preserved jellyfishes from the middle Cambrian. PloS One 2:e1121.

Cartwright, P., Nawrocki, A.M., 2010. Character evolution in Hydrozoa (phylum Cnidaria). *Integr Comp Biol* 50, 456–472.

Cartwright P, Travert MK, Sanders SM (2020) The evolution of development of coloniality of hydrozoans. *J Exp Zool* DOI: 10.1002/jez.b.22996

Collins AG, Schuchert P, Marwues, AC, Jankowski T, Medina M, Schierwater B (2006) Medusozoan phylogeny and character evolution clarified by new large and small subunit rDNA data and assessment of the utility of phylogenetic mixture models. *Systematic Biology*, 55, 97-115.

Chapman JA, Kirkness EF, Simakov O, Hampson SE, Mitros T, Weinmaier T, Rattei T, Balasubramanian PG, Borman J, Busam D, Disbennett K, Pfannkoch C, Sumin N, Sutton GG, Viswanathan LD, Walenz B, Goodstein DM, Hellsten U, Kawashima T, Prochnik SE, Putnam NH, Shu S, Blumberg B, Dana CE, Gee L, Kibler DF, Law L, Lindgens D, Martinez DE, Peng J, Wigge PA, Bertulat B, Guder C, Nakamura Y, Ozbek S, Watanabe H, Khalturin K, Hemmrich G, Franke A, Augustin R, Fraune S, Hayakawa E, Hayakawa S, Hirose M, Hwang JS, Ikeo K, Nishimiya-Fujisawa C, Ogura A, Takahashi T, Steinmetz PRH, Zhang X, Aufschnaiter R, Eder M-K, Gorny A-K, Salvenmoser W, Heimberg AM, Wheeler BM, Peterson KJ, Böttger A, Tischler P, Wolf A, Gojobori T, Remington KA, Strausberg RL, Venter JC, Technau U, Hobmayer B, Bosch TCG, Holstein TW, Fujisawa T, Bode HR, David CN, Rokhsar DS, Steele RE (2010) The dynamic genome of *Hydra*. *Nature* 464:592-596.

Daly M, Brugler MR, Cartwright P, Collins AG, Dawson MN, Fautin DG, France SC, McFadden CS, Opresko DM, Rodriguez E, Romano SL, Stake JL (2007) The phylum Cnidaria: a review of phylogenetic patterns and diversity 300 years after Linnaeus. *Zootaxa* 1668:127-182.

Erickson KL, Pentico1 A, Quattrini AM, McFadden CS (2020) New approaches to species delimitation and population structure of corals: two case studies using ultra-conserved elements and exons. *Molecular Ecology Resources* DOI: 10.1111/1755-0998.13241.

Erwin DH (2020) The origin of animal body plans: a view from fossil evidence and the regulatory genome. *Development* 147:dev182899.

Fourment M, Magee AF, Whidden C, Bilge A, Matsen FA, Minin VN (2020) 19 dubious ways to compute the marginal likelihood of a phylogenetic tree topology. *Systematic Biology* 69:209–220.

Green MR, Sambrook J (2012) *Molecular Cloning – A laboratory manual.* Cold Spring Harbor Press, Cold Spring Harbor, NY, 2028pp.

Han J, Zang X, Komiya T (2016) *Integrated evolution of cnidarians and oceanic geochemistry before and during the Cambrian explosion.* In: The Cnidaria, Past, Present, and Future (eds. Goffredo S, Dubinsky Z), 15-29.

Hasegawa M, Kishino H. (1994) Accuracies of the simple methods for estimating the bootstrap probability of a maximum-likelihood tree. *Mol Biol Evol* 11:142-145.

Jeffreys, H. (1961). *Theory of probability (3rd ed.)*. Oxford University Press, New York, NY, 472pp.

Johnson MG, Gardner EM, Liu Y, Medina R, Goffinet B, Shaw AJ, Zerega NJC, Wickett NJ (2016) HybPiper: Extracting coding sequence and introns for phylogenetics from high-throughput sequencing reads using target enrichment. *Applications in Plant Sciences*, 4.

Kass RE, Raftery AE (1995) Bayes factors. *Journal of the American Statistical Association* 430:773-795.

Katoh, K., & Standley, D. M. (2013). MAFFT multiple sequence alignment software version 7: improvements in performance and usability. *Mol Biol Evol* 30:772–780.

Kayal E, Bentlage B, Cartwright P, Yanagihara AA, Lindsay DJ, Hopcroft RR, Collins AG (2015) Phylogenetic analysis of higher-level relationships within Hydroidolina (Cnidaria: Hydrozoa) using mitochondrial genome data and insight into their mitochondrial transcription. *PeerJ* 3:e1403.

Kayal E, Bentlage B, Pankey MS, Ohdera AH, Medina M, Plachetzki DC, Collins AG, Ryan JF (2018) Phylogenomics provides a robust topology of the major cnidarian lineages and insights on the origins of key organismal traits. *BMC Evolutionary Biology* 18:68.

Kishino H, Miyata T, Hasegawa M (1990) Maximum-likelihood inference of protein phylogeny and the origin of chloroplasts. *J Mol Evol* 31:151-160.

Lanfear, R., Calcott, B., Kainer, D., Mayer, C., & Stamatakis, A. (2014). Selecting optimal partitioning schemes for phylogenomic datasets. *BMC Evolutionary Biology* 14: 82.

Lanfear, R., Frandsen, P. B., Wright, A. M., Senfeld, T., Calcott, B. (2017) PartitionFinder 2: new methods for selecting partitioned models of evolution for molecular and morphological phylogenetic analyses. *Mol Biol Evol* 34:772-773.

Lartillot N, Philippe H (2004) A Bayesian mixture model for across-site heterogeneities in the amino-acid replacement process. *Mol Biol Evol* 21:1095-1109.

Lartillot N, Rodrigue N, Stubbs D, Richer J (2013) PhyloBayes MPI: Phylogenetic reconstruction with infinite mixtures of profiles in a parallel environment. *Systematic Biology* 62:611–615.

Le, SQ, Gascuel, O. 2008 An improved general amino-acid replacement matrix. *Mol Biol Evol* 25, 1307–1320.

Morey RD, Romeijn J-W, Rouder JN (2016) The philosophy of Bayes factors and the quantification of statistical evidence. *Journal of Mathematical Psychology* 72:6-18.

Ohdera A, Ames CL, Dikow RB, Kayal E, Chiodin M, Busby B, La S, Pirro S, Collins AG, Medina M, Ryan JF. (2019) Box, stalked, and upside-down? Draft genomes from diverse jellyfish (Cnidaria, Acraspeda) lineages: *Alatina alata* (Cubozoa), *Calvadosia cruxmelitensis* (Staurozoa), and *Cassiopea xamachana* (Scyphozoa). *GigaScience* 8:giz069.

Putnam NH, Srivastava M, Hellsten U, Dirks B, Chapman J, Salamov A, Terry A, Shapiro A, Lindquist E, Kapitonov VV, Jurka J, Genikhovich G, Grigoriev IV, Lucas SM, Steele RE, Finnerty JR, Technau U, Martindale MQ, Rokhsar DS (2007) Sea anemone genome reveals ancestral eumetazoan gene repertoire and genomic organization. *Science* 317:86-94.

Quattrini AM, Faircloth BC, Dueñas LF, Bridge TCL, Brugler MR, Calixto-Botía IF, DeLeo DM, Forêt S, Herrera S, Lee SMY, Miller DJ, Prada C, Rádis-Baptista G, Ramírez-Portilla C, Sánchez JA, Rodríguez E, McFadden CS (2018) Universal target-enrichment baits for anthozoan (Cnidaria) phylogenomics: New approaches to long-standing problems. *Mol Ecol Resour* 18:281-295.

Rota-Stabelli O, Yang Z, Telford MJ. (2009) MtZoa: a general mitochondrial amino acid substitutions model for animal evolutionary studies. *Mol Phylogenet Evol*. 52:268-272.

Rubinoff D, Holland BS (2005) Between two extremes: mitochondrial DNA is neither the Panacea nor the nemesis of phylogenetic and taxonomic inference. *Systematic Biology* 54:952-961.

Schuchert, P. (2020). World Hydrozoa Database. Accessed at http://www.marinespecies.org/hydrozoa on 2020-09-15. DOI:10.14284/357

Schwarz G (1978) Estimating the dimension of a model. *The Annals of Statistics* 6:461-464.

Shimodaira, H. (2002) An approximately unbiased test of phylogenetic treeselection. *Systematic Biology* 51:492-508.

Shimodaira, H. and Hasegawa, M. (2001) CONSEL: for assessing the confidence of phylogenetic tree selection. *Bioinformatics* 17:1246-1247.

Shinzato, C., Shoguchi, E., Kawashima, T., Hamada, M., Hisata, K., Tanaka, M., Fujie, M., Fujiwara, M., Koyanagi, R., Ikuta, T., Fujiyama, A., Miller, D. J., and Satoh, N. (2011) Using the *Acropora digitifera* genome to understand coral responses to environmental change. *Nature* 476:320-323.

Sober E (2008) *Evidence and Evolution: The logic behind the science.* Cambridge University Press, Cambridge, UK, pp. 412.

Slater GS, Birney E (2005) Automated generation of heuristics for biological sequence comparison. *BMC Bioinformatics* 6:31.

Smit AFA, Hubley R, Green P. (2013-2015) *RepeatMasker Open-4.0* <http://www.repeatmasker.org>.

Stamatakis A (2006) RAxML-VI-HPC: maximum likelihood-based phylogenetic analyses with thousands of taxa and mixed models, *Bioinformatics* 22:2688–2690.

Talavera, G., Castresana, J. (2007) Improvement of phylogenies after removing divergent and ambiguously aligned blocks from protein sequence alignments. *Systematic Biology* 56: 564–577.

Valentine JW, Jablonski D, Erwin DH (1999) Fossils, molecules and embryos: new perspectives on the Cambrian explosion. *Development* 126:851-859.

Wiens JJ, Morrill MC (2011) Missing data in phylogenetic analysis: reconciling results from simulations and empirical data. *Systematic Biology* 60:719-731.

Whelan, S. & Goldman, N. 2001 A general empirical model of protein evolution derived from multiple protein families using a maximum-likelihood approach. *Mol Biol Evol*18,691–699.

Zapata F, Goetz FE, Smith SA, Howison M, Siebert S, Church SH, Sanders SM, Ames CL, McFadden CS, France SC, Daly M, Collins AG, Haddock SH, Dunn CW, Cartwright P (2015) Phylogenomic analyses support traditional relationships within Cnidaria. *PLoS One* 10:e0139068.

Tables

Table 1 Reference genomes used for verification of candidate baits.

Taxon	Source
Medusozoa: Hydrozoa: *Hydra magnipapillata*	Chapman et al., 2010
Medusozoa: Cubozoa: *Alatina alata*	Ohdera et al., 2019
Medusozoa: Staurozoa: *Calvadosia cruxmelitensis*	Ohdera et al., 2019
Anthozoa: Pentalucea: *Renilla* sp.	Ohdera et al., 2019
Anthozoa: Scleractinia: *Acropora digitifera*	Shinzato et al., 2011
Anthozoa: Actiniaria: *Nematostella vectensis*	Putnam et al., 2007

Table 2 Species and sequence data sampled for phylogenetic analyses. Data for species in bold were generated in this study. For each species, the number of loci and amino acid residues included in the final concatenated 134 locus alignment are provided. NCBI: National Center for Biotechnology Information; USNM: National Museum of Natural History, Smithsonian Institution; UOGCVC: University of Guam Coral Voucher Collection.

		Taxon	Voucher/Reference	Loci	Residues	NCBI Accession
Hydroidolina	Capitata	***Zancleopsis tentaculata***	**USNM1622168**	**12**	**1,103**	**MW272249 – MW272260**
		Millepora dichotoma	**UOGCVC947**	**6**	**726**	**MW272119 – MW272124**
		Pennaria disticha	**USNM1622068**	**47**	**4,403**	**MW272261 – MW272307**
	Filifera I	***Myrionema hargitti***	**USNM1622176**	**22**	**2,005**	**MW272227 – MW272248**
	Filifera II	***Proboscidactyla* sp.**	**USNM1622170**	**5**	**448**	**MW272435 – MW272439**
	Leptothecata	***Dynanema crisioides***	**USNM1622069**	**62**	**6,173**	**MW272032 – MW272093**
		Nemalecium lighti	**USNM1622067**	**54**	**5,256**	**MW272125 – MW272178**
		Aglaophenia parvula	**USNM1621045**	**39**	**3,890**	**MW272179 – MW272217**
		Kirchenpaueria halecioides	**USNM1622065**	**25**	**2,548**	**MW272094 – MW272118**
		***Kirchenpaueria* sp.**	**USNM1621044**	**84**	**8,018**	**MW272308 – MW272391**
		***Octophialucium* sp.**	**USNM1622151**	**40**	**3,334**	**MW271992 – MW272031**
		Clytia hemispherica	Kayal et al., 2018	26	4,266	
	Filifera III	*Podocoryne carnea*	Kayal et al., 2018	109	16,709	
		Podocoryne martinicana	**USNM1622132**	**9**	**1,077**	**MW272218 – MW272226**
		Hydractinia symbiolongicarpus	Kayal et al., 2018	104	16,411	
		Hydractinia polyclina	Kayal et al., 2018	107	16,950	
	Filifera IV	***Merga violacea***	**USNM1622162**	**10**	**831**	**MW271982 – MW271991**

Outgroup	Siphonophorae	***Athorybia rosacea***	**USNM1622138**	**6**	**871**	**MW272429 – MW272434**
		Agalma elegans	Kayal et al., 2018	99	15,170	
		Nanomia bijuga	Kayal et al., 2018	96	14,339	
		Craseoa lathetica	Kayal et al., 2018	89	13,177	
		Abylobsis tetragona	Kayal et al., 2018	95	14,370	
		Physalia physalis	Kayal et al., 2018	105	15,455	
	Aplanulata	*Hydra magnipapillata*	Kayal et al., 2018	94	14,171	
		Hydra vulgaris	Kayal et al., 2018	105	16,187	
		Hydra oligactis	Kayal et al., 2018	64	8,342	
		Hydra viridissima	Kayal et al., 2018	70	9,237	
		Ectopleura larynx	Kayal et al., 2018	106	16,688	
	Trachylina	*Craspedacusta sowerbii*	Kayal et al., 2018	116	18,413	
		Aglaura hemistoma	**USNM1622142**	**8**	**925**	**MW271974 – MW271981**
		Solmundaegina nematophora	**USNM1284330**	**6**	**324**	**MW271968 – MW271973**
		Aegina citrea	Kayal et al., 2018	69	9,713	
	Cubozoa	*Alatina alata*	Kayal et al., 2018	113	17,918	
		Tripedalia cystophora	Kayal et al., 2018	34	4,088	
	Scyphozoa	*Periphylla periphylla*	Kayal et al., 2018	55	6,980	
		Atolla vanhoeffeni	Kayal et al., 2018	85	12,468	
		Chrysaora chesapeakei	**USNM1454941**	**37**	**3,145**	**MW272392 – MW272428**
		Cyanea capillata	Kayal et al., 2018	37	4,503	
		Stomolophus meleagris	Kayal et al., 2018	103	15,551	
		Cassiopea sp.	Kayal et al., 2018	93	12,888	
		Aurelia aurita	Kayal et al., 2018	111	17,342	
	Staurozoa	***Haliclystus auricula***	**USNM1621043**	**17**	**1,406**	**MW271951 – MW271967**
		Craterolophus convolvulus	Kayal et al., 2018	94	12,821	
		Calvadosia cruxmelitensis	Kayal et al., 2018	109	16,800	

Table 3 Log likelihood of maximum likelihood inferences under different topological constraints (see Fig. 3). Likelihood ratios were calculated to compare alternate tree hypotheses to the null, T_0 (cf. Cartwright and Nawrocki, 2010). The approximately unbiased test (AU) was used to test the null hypothesis that all tree topologies have the same log likelihood. Tree topology fit to the alignment data was evaluated using the posterior probability of the Bayesian Information Criterion (BIC).

Constraint	Log Likelihood	Likelihood Ratio	AU	BIC Posterior
T_0	-375844.52	-	2e-4	4e-46
T_1	-375944.68	-200.32	4e-4	1e-89
T_2	-375741.33	206.38	**0.54**	**0.282**
T_3	-375740.41	208.22	**0.60**	**0.718**
T_4	-375749.48	190.08	**0.31**	8e-5
T_5	-375759.35	170.35	**0.14**	4e-9

Figures

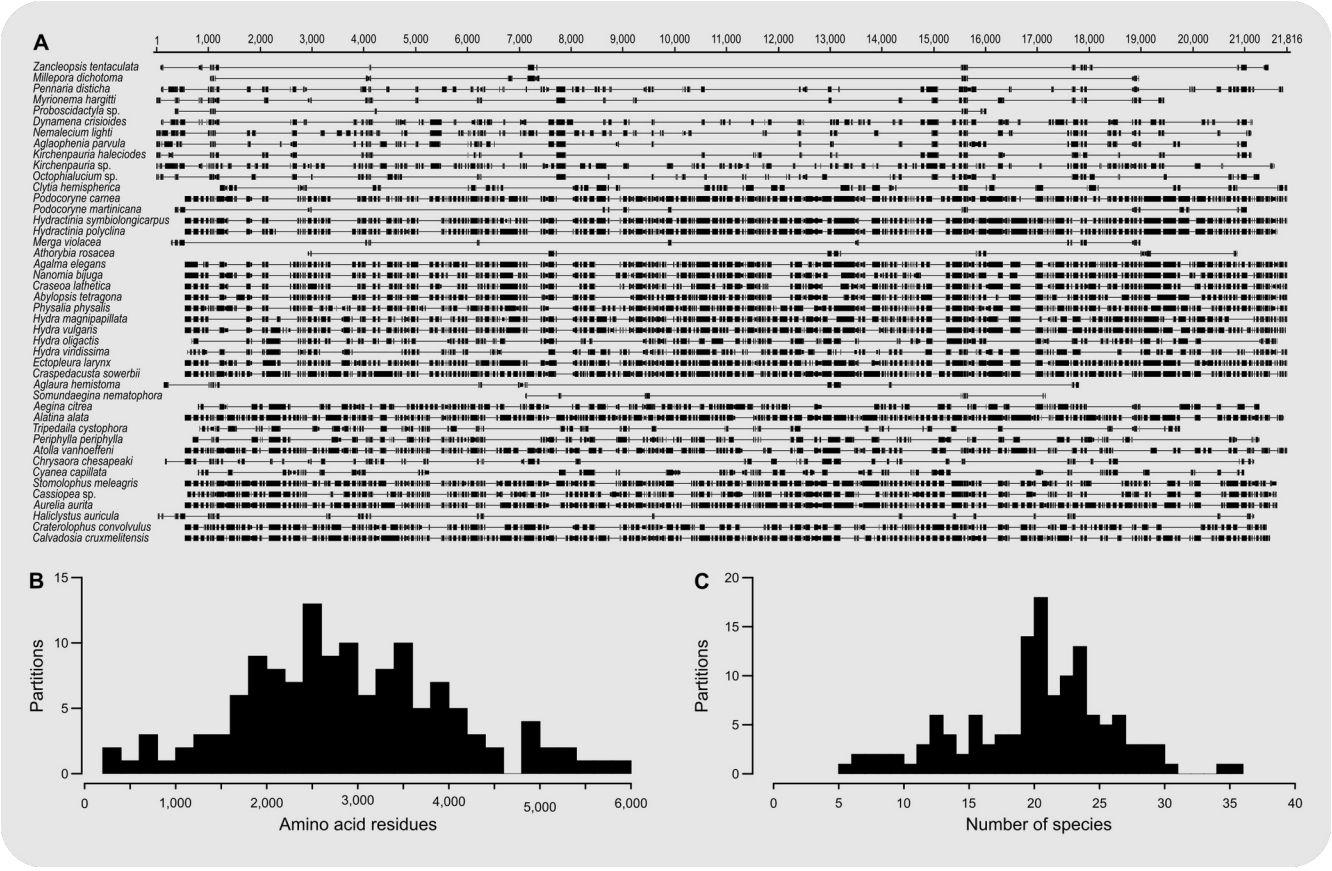

Fig. 1 A) Alignment of the 134 amino acid residue partitions; B) total number of amino acid residues contained in each alignment partition; C) number of species included in each alignment partition.

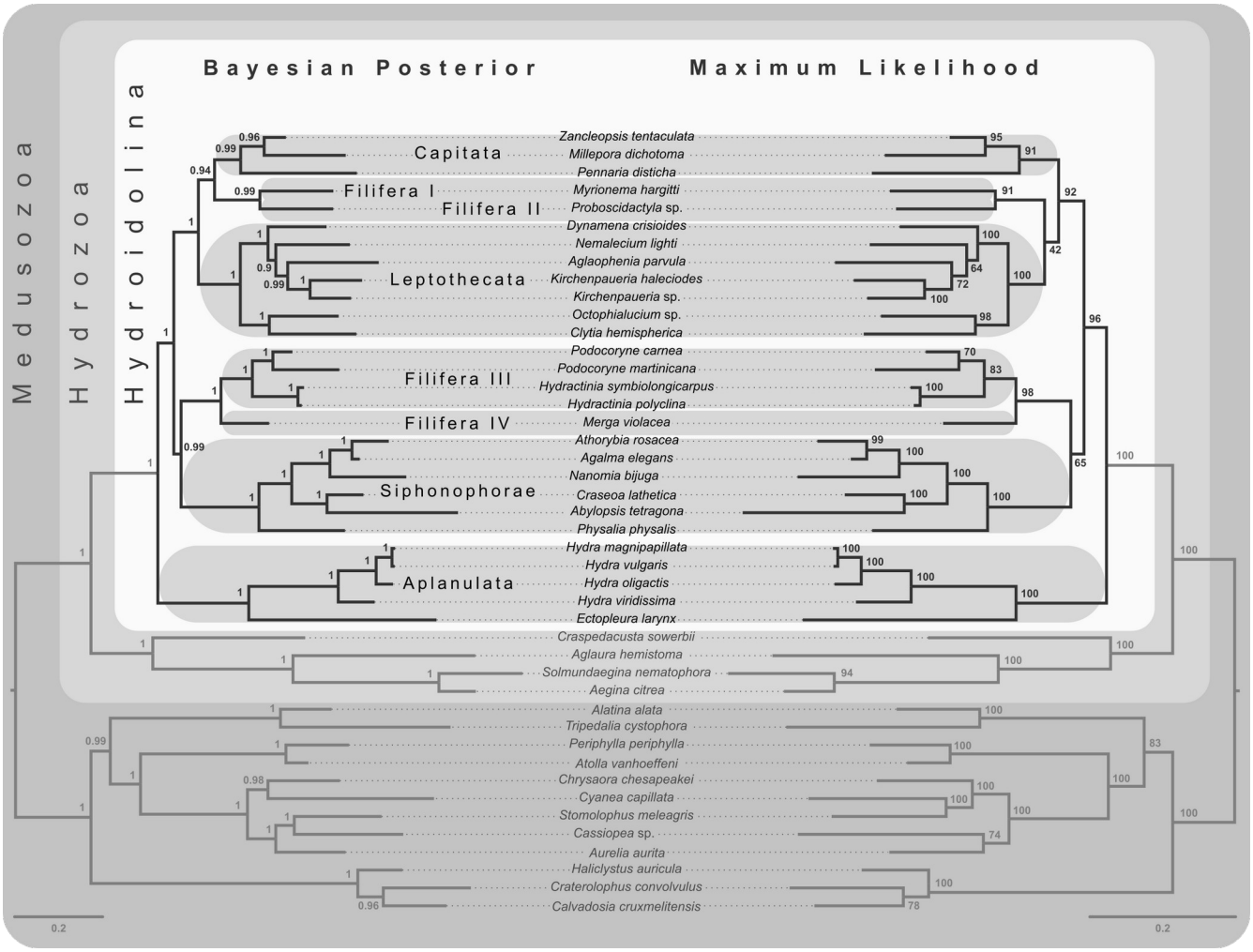

Fig. 2 Majority rule consensus of Bayesian phylogenetic inference under the CAT-GTR model (left side) with posterior probabilities given at each node. Maximum likelihood phylogeny (right side) was inferred from a partitioned analysis under the LG, WAG, and MtZoa models. Node support values represent the summary of 681 non-parametric maximum likelihood bootstrap searches. Scale bars indicate the number of substitutions per site.

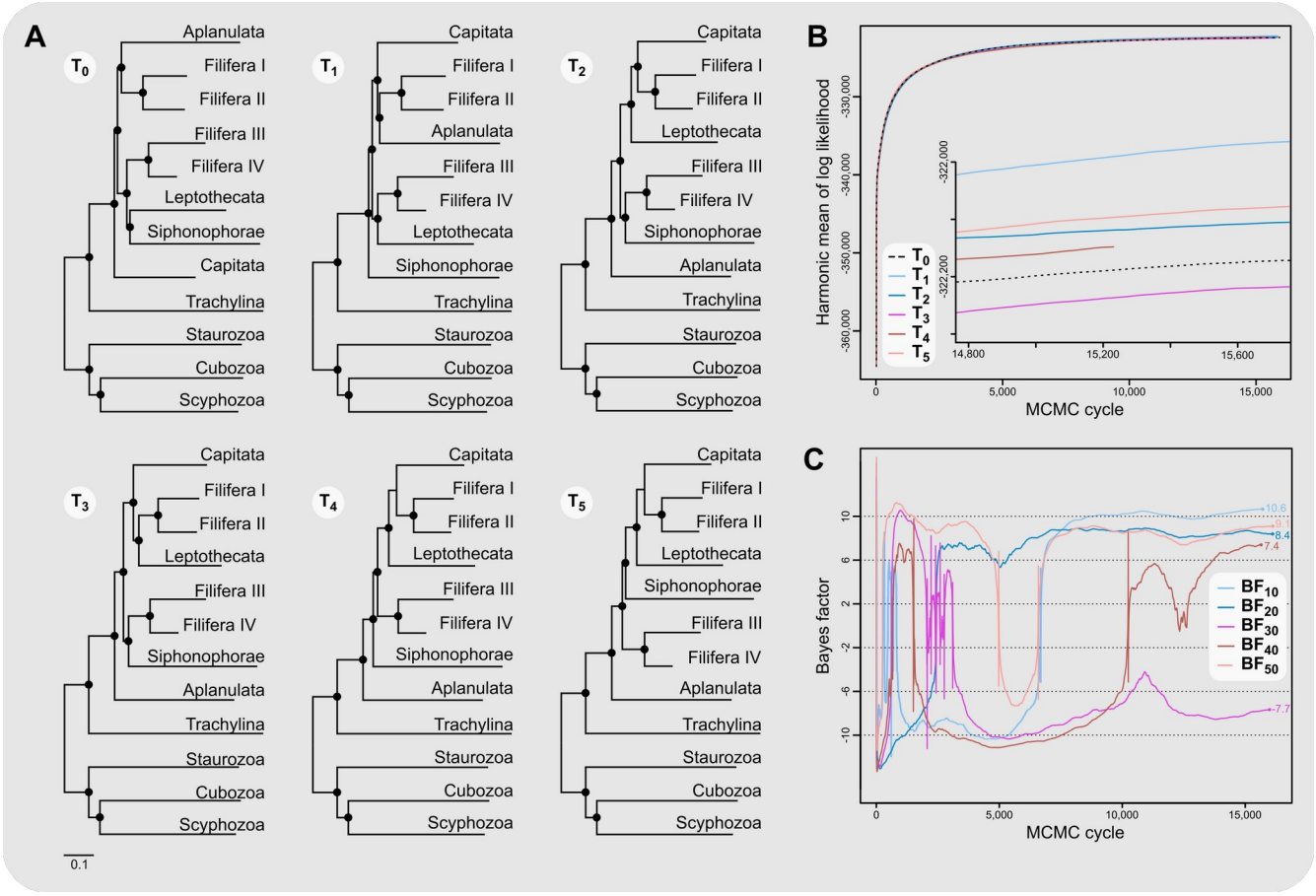

Fig. 3 A) Phylogenetic tree topologies inferred using maximum likelihood searches. Shallow nodes were collapsed, and species labels remove for legibility. Nodes that were constrained are indicated by black solid circles; scale bar indicates the number of substitutions per site. B) Harmonic means of the posterior from constrained Bayesian inferences. Constraints (priors) correspond to the topologies shown in (A). C) Bayes factors for pairwise comparisons between T_0 and alternate hypotheses (A). Negative Bayes factors provide evidence for T_0 while positive Bayes factors indicate evidence against T_0, providing support for the alternate hypothesis. A Bayes factor between -2 and 2 indicates lack of evidence or no evidence favoring one hypothesis over the other, Bayes factors in the range of 2 to 6 (-2 to -6) provide some evidence, 6 to 10 (-6 to -10) strong evidence, and Bayes factors > 10 (< -10) very strong evidence for one hypothesis compared to the other.

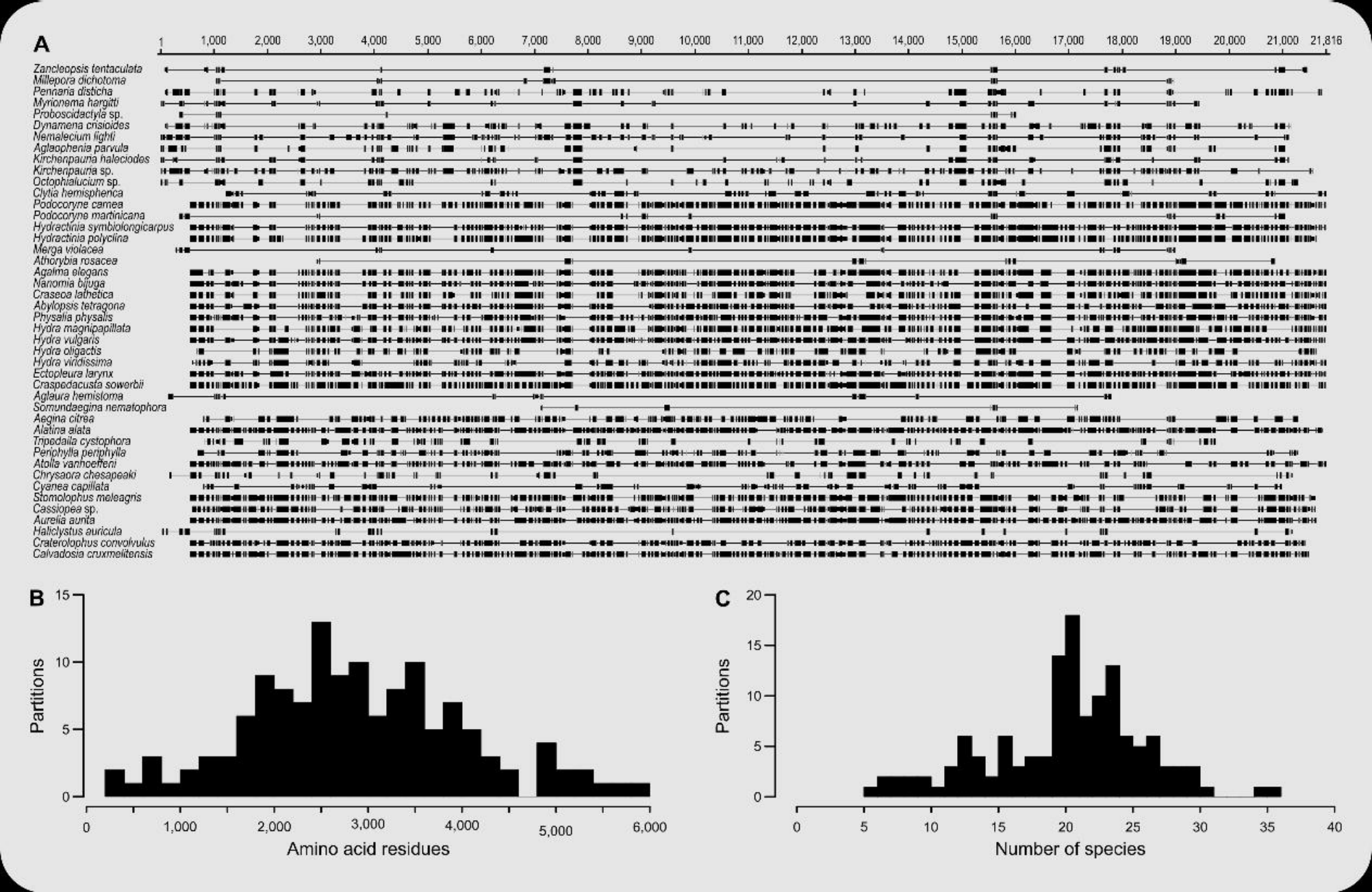
A
1
1,000
2,000
3,000
4,000
5,000
6,000
7,000
8,000
9,000
10,000
11,000
12,000
13,000
14,000
15,000
16,000
17,000
18,000
19,000
20,000
21,000
21,816
Zancleopsis tentaculata
Millepora dichotoma
Pennaria disticha
Myrionema hargitti
Proboscidactyla sp.
Dynamena crisioides
Nemalecium lighti
Aglaophenia parvula
Kirchenpauna halecioides
Kirchenpauna sp.
Octophialucium sp.
Clytia hemisphenica
Podocoryne carnea
Podocoryne martinicana
Hydractinia symbiolongicarpus
Hydractinia polyclina
Merga violacea
Athorybia rosacea
Agalma elegans
Nanomia bijuga
Craseoa lathetica
Abylopsis tetragona
Physalia physalis
Hydra magnipapillata
Hydra vulgaris
Hydra oligactis
Hydra viridissima
Ectopleura larynx
Craspedacusta sowerbii
Aglaura hemistoma
Somundaegina nematophora
Aegina citrea
Alatina alata
Tripedalia cystophora
Periphylla periphylla
Atolla vanhoeffeni
Chrysaora chesapeaki
Cyanea capillata
Stomolophus meleagris
Cassiopea sp.
Aurelia aurita
Haliclystus auricula
Craterolophus convolvulus
Calvadosia cruxmelitensis
B
Partitions
0
5
10
15
0
1,000
2,000
3,000
4,000
5,000
6,000
Amino acid residues
C
Partitions
0
5
10
15
20
0
5
10
15
20
25
30
35
40
Number of species

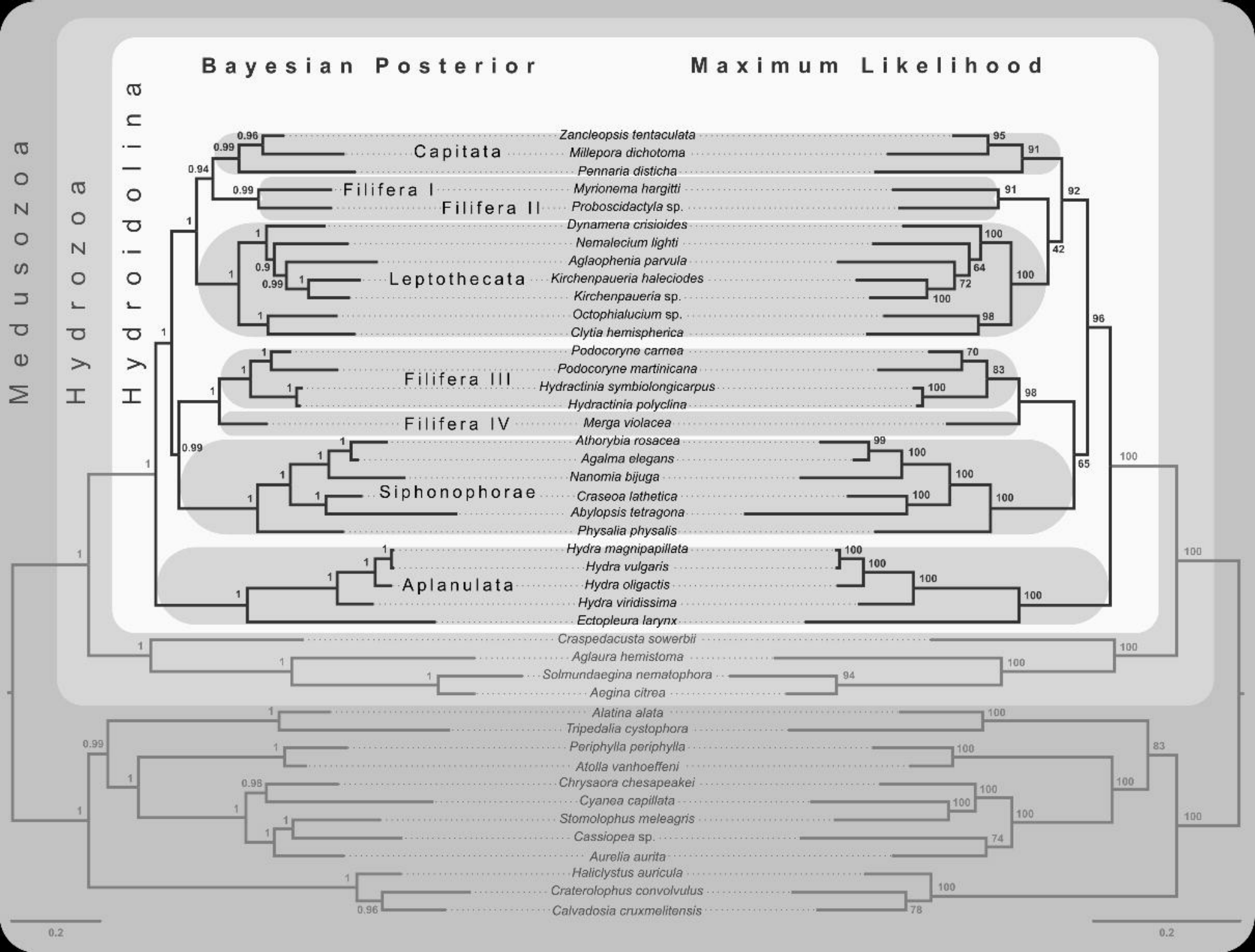
Bayesian Posterior
Maximum Likelihood
Medusozoa
Hydroidolina
Capitata
Filifera I
Filifera II
Leptothecata
Filifera III
Filifera IV
Siphonophorae
Aplanulata
Zancleopsis tentaculata
Millepora dichotoma
Pennaria disticha
Myrionema hargitti
Proboscidactyla sp.
Dynamena crisioides
Nemalecium lighti
Aglaophenia parvula
Kirchenpaueria haleciodes
Kirchenpaueria sp.
Octophialucium sp.
Clytia hemispherica
Podocoryne carnea
Podocoryne martinicana
Hydractinia symbiolongicarpus
Hydractinia polyclina
Merga violacea
Athorybia rosacea
Agalma elegans
Nanomia bijuga
Craseoa lathetica
Abylopsis tetragona
Physalia physalis
Hydra magnipapillata
Hydra vulgaris
Hydra oligactis
Hydra viridissima
Ectopleura larynx
Craspedacusta sowerbii
Aglaura hemistoma
Solmundaegina nematophora
Aegina citrea
Alatina alata
Tripedalia cystophora
Periphylla periphylla
Atolla vanhoeffeni
Chrysaora chesapeakei
Cyanea capillata
Stomolophus meleagris
Cassiopea sp.
Aurelia aurita
Haliclystus auricula
Craterolophus convolvulus
Calvadosia cruxmelitensis
0.2
0.2

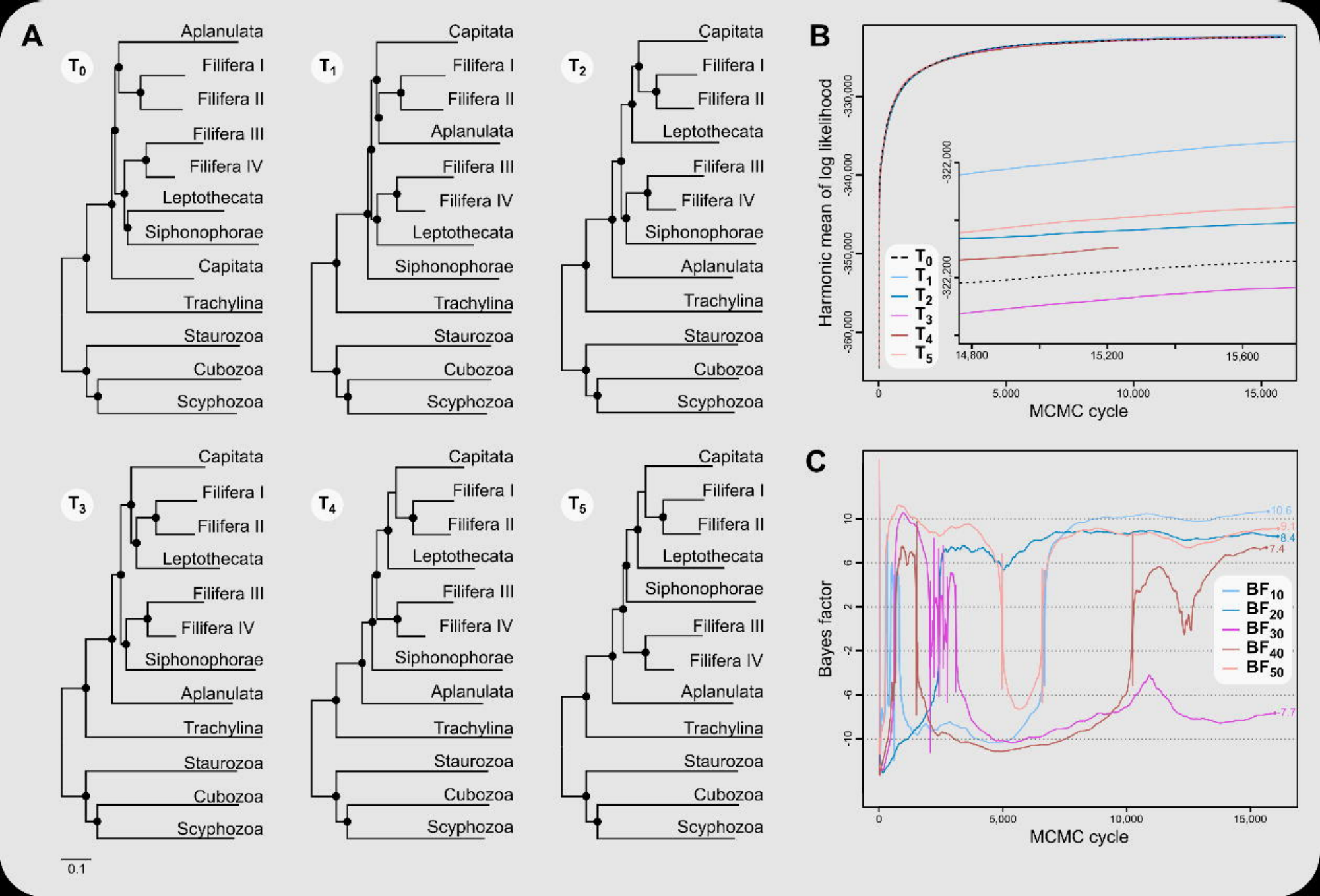
A
T0
Aplanulata
Filifera I
Filifera II
Filifera III
Filifera IV
Leptothecata
Siphonophorae
Capitata
Trachylina
Staurozoa
Cubozoa
Scyphozoa
T1
Capitata
Filifera I
Filifera II
Aplanulata
Filifera III
Filifera IV
Leptothecata
Siphonophorae
Trachylina
Staurozoa
Cubozoa
Scyphozoa
T2
Capitata
Filifera I
Filifera II
Leptothecata
Filifera III
Filifera IV
Siphonophorae
Aplanulata
Trachylina
Staurozoa
Cubozoa
Scyphozoa
T3
Capitata
Filifera I
Filifera II
Leptothecata
Filifera III
Filifera IV
Siphonophorae
Aplanulata
Trachylina
Staurozoa
Cubozoa
Scyphozoa
T4
Capitata
Filifera I
Filifera II
Leptothecata
Filifera III
Filifera IV
Siphonophorae
Aplanulata
Trachylina
Staurozoa
Cubozoa
Scyphozoa
T5
Capitata
Filifera I
Filifera II
Leptothecata
Siphonophorae
Filifera III
Filifera IV
Aplanulata
Trachylina
Staurozoa
Cubozoa
Scyphozoa
0.1
B
Harmonic mean of log likelihood
-330,000
-340,000
-350,000
-360,000
-322,000
-322,200
14,800
15,200
15,600
T0
T1
T2
T3
T4
T5
0
5,000
10,000
15,000
MCMC cycle
C
Bayes factor
10
6
2
-2
-6
-10
10.6
9.1
8.4
7.4
7.7
BF10
BF20
BF30
BF40
BF50
0
5,000
10,000
15,000
MCMC cycle